Journal of Medicinal Chemistry

Article

pubs.acs.org/jmc

Total Synthesis of AMF-26, an Antitumor Agent for Inhibition of the Golgi System, Targeting ADP-Ribosylation Factor 1

Isamu Shiina,*[,†] Yuma Umezaki,[†] Yoshimi Ohashi,[‡] Yuta Yamazaki,[†] Shingo Dan,[‡] and Takao Yamori[‡]

[†]Department of Applied Chemistry, Faculty of Science, Tokyo University of Science, 1-3 Kagurazaka, Shinjuku-ku, Tokyo 162-8601, Japan

[‡]Division of Molecular Pharmacology, Cancer Chemotherapy Center, Japanese Foundation for Cancer Research, 3-8-31 Ariake, Koto-ku, Tokyo 135-8550, Japan

Supporting Information

ABSTRACT: An effective method for the total synthesis of **1** (AMF-26), a potentially promising new anticancer drug that disrupts the Golgi system by inhibiting the ADP-ribosylation factor 1 (Arf1) activation, has been developed for the first time. The construction of the chiral linear precursor (a key to the synthesis) was achieved by the asymmetric aldol reaction followed by the computer-assisted predictive stereoselective intramolecular Diels–Alder reaction. The global antitumor activity of the totally synthetic **1** against a variety of human cancer cells was assessed using a panel of 39 human cancer cell lines (JFCR39), and it was shown that the synthetic **1** strongly inhibited the growth of several cancer cell lines at concentrations of less than 0.04 μM. Biological assays of novel derivatives, **26** and **31**, which have different side-chains at the C-4 positions in the $\Delta^{1,2}$-octalin backbone, disclosed the importance of the suitable structure of the side-chain containing conjugated multidouble bonds.

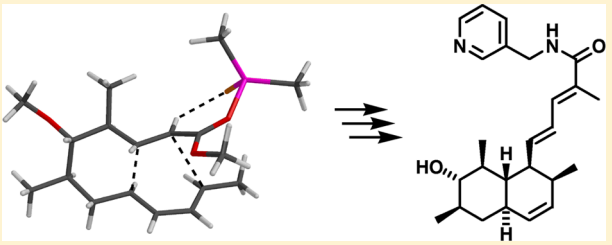

INTRODUCTION

(2*E*,4*E*)-5-((3*S*,4*S*,4a*S*,5*S*,6*S*,7*R*,8a*R*)-3,4,4a,5,6,7,8,8a-Octahydro-6-hydroxy-3,5,7-trimethylnaphthalen-4-yl)-2-methyl-*N*-((pyridin-3-yl)methyl)penta-2,4-dienamide (AMF-26) (**1**)[1] has been semisynthesized from (2*E*,4*E*)-5-((3*S*,4*S*,4a*S*,5*S*,6*S*,7*R*,8a*R*)-3,4,4a,5,6,7,8,8a-octahydro-6-hydroxy-3,5,7-trimethylnaphthalen-4-yl)-2-methylpenta-2,4-dienoic acid (AMF-14) (**2**),[2] a natural product isolated from the genus *Trichoderma* NFS-932 by Nippon Shinyaku Co., Ltd., in 2005 (Figure 1). The

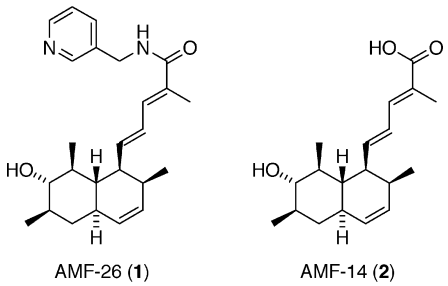

Figure 1. Structures of AMF-26 (**1**) and AMF-14 (**2**).

compound **1** is a potentially promising new anticancer drug lead because its oral administration to female nude mice induced complete regression of human breast cancer BSY-1 xenografts in vivo.[2] It was revealed that **1** induced Golgi disruption, apoptosis, and cancer-cell growth inhibition through a mechanism for preventing the ADP-ribosylation factor 1 (Arf1) activation introduced by Ohashi and Yamori et al.[2] Arf1 has an important role in mediating vesicular transport. Recently, protein–protein interaction, such as the activation of Arf1 by its guanine nucleotide exchange factor (ArfGEF), has become a very attractive new target for providing effective therapeutic agents, including novel anticancer drugs.[3] From computer modeling, it is postulated that **1** binds to the contact surface of the Arf1–Sec7 domain where brefeldin A bound. Brefeldin A was first introduced as the inhibitor of the Arf1–ArfGEF interaction;[4−6] however, brefeldin A has not progressed beyond the preclinical stage of drug development because of its poor bioavailability.[6a,7] Therefore, **1**, a new Golgi inhibitor targeting Arf1 activation, can be one of the first candidates for a new type of medicine for cancer treatment in clinical use. Furthermore, another biological activity of **1**, angiogenesis inhibition of the vascular endothelial growth factor (VEGF) receptor phosphorylation and NF-κB signaling, has been investigated by Watari and Nakamura et al.[8]

In this study, we report the first total synthesis of **1** using the asymmetric aldol reaction for constructing the chiral linear precursor and computer-assisted predictive stereoselective intramolecular Diels–Alder (IMDA) reaction to provide the core structure of the multisubstituted octahydronaphthalene.

TOTAL SYNTHESIS OF AMF-26

Retrosynthetic Analysis of 1 via IMDA Reaction. Scheme 1 outlines our designed asymmetric synthesis of **1**, including the three following notable methodologies: (i) the diastereoselective

Received: September 18, 2012
Published: December 6, 2012

   dx.doi.org/10.1021/jm301695c | J. Med. Chem. 2013, 56, 150−159

Scheme 1. Retrosynthetic Analysis of 1

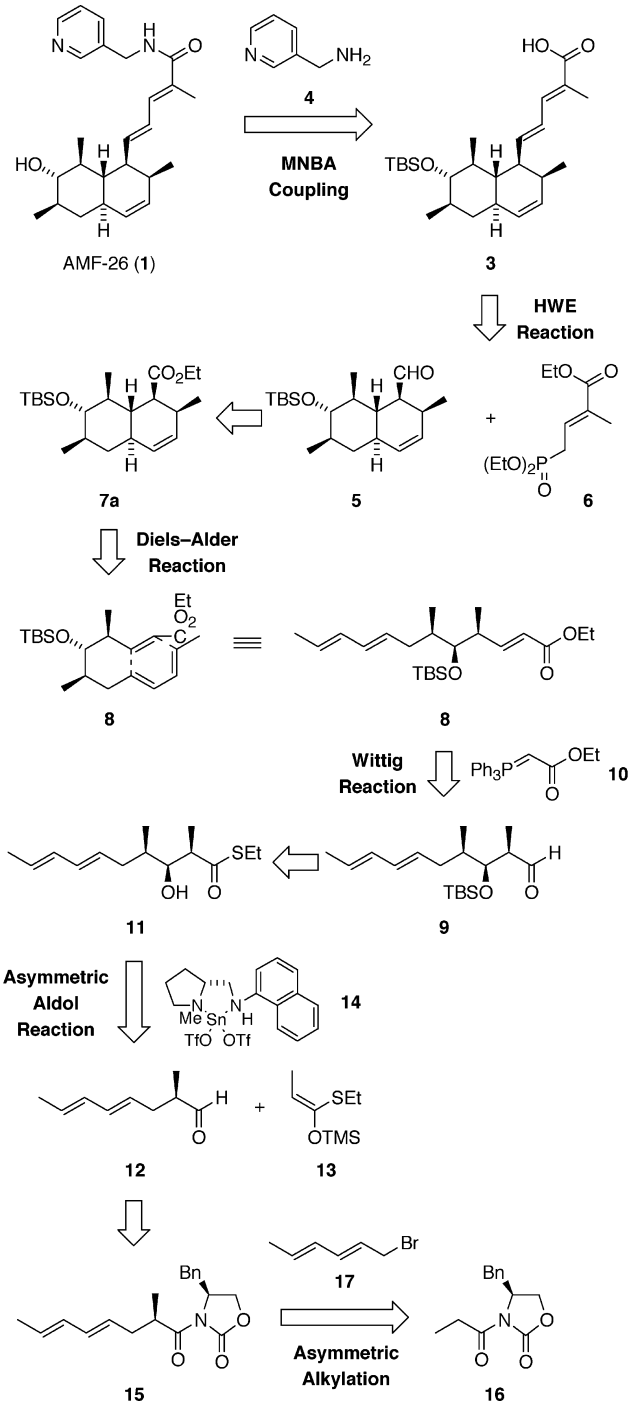

Evans' alkylation[9] of the chiral oxazolidinone **16** with (*E*,*E*)-1-bromohexa-2,4-diene (**17**) to form a chiral diene **15**, (ii) the enantioselective Mukaiyama aldol reaction[10] of an aldehyde **12** with ketene silyl acetal (KSA) **13** to form an *α*,*β*,*γ*-trisubstituted chiral thioester **11**, and (iii) the diastereoselective IMDA reaction[11] of the chiral linear ester **8** to form octahydronaphthalene **7a**. Other transformations, such as the Wittig reaction of an aldehyde **9** with an ylide **10** to provide an ester **8**, the HWE (Horner–Wadsworth–Emmons) reaction of an aldehyde **5** with phosphate **6** to provide a carboxylic acid **3**, and the MNBA coupling reaction[12] of **3** with 3-pyridylmethylamine (**4**) to afford the corresponding amide, might be successfully carried out for the preparation of the basic skeleton of the target molecule **1** in this plan.

Asymmetric Synthesis of Chiral Linear Ester 8 and Prediction of the Stereoselectivity in the IMDA Reaction of 8M to Form $\Delta^{1,2}$-Octalins 7Ma–d. First, Evans' chiral oxazolidinone **16**[9] was converted into the sodium enolate by the reaction with NaHMDS, followed by the treatment with **17**[13] in the presence of tetrabutylammonium iodide (TBAI) to diastereoselectively form diene **15** (Scheme 2). Removal of the chiral auxiliary

Scheme 2. Preparation of the Key Chiral Linear Ester 8 Intermediate[a]

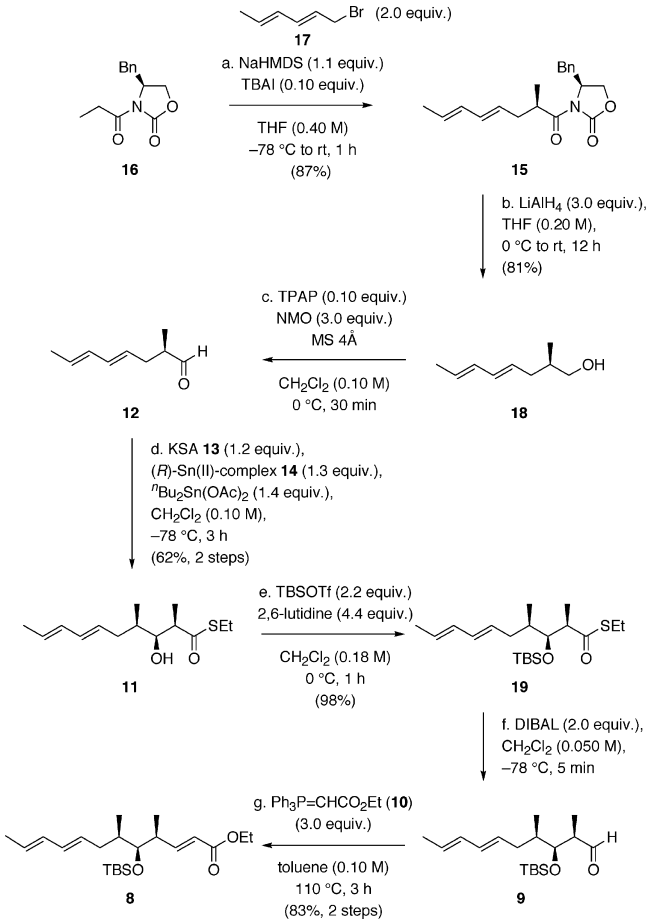

[a]Reagents and conditions: (a) NaHMDS, THF, −78 °C, 15 min, and then bromide **17**, TBAI, rt, 1 h, 87%; (b) $LiAlH_4$, THF, 0 °C to rt, 12 h, 81%; (c) TPAP, NMO, 4-Å molecular sieves, CH_2Cl_2, 0 °C, 30 min; (d) KSA **13**, (*R*)-Sn(II)-complex **14**, $^nBu_2Sn(OAc)_2$, CH_2Cl_2, −78 °C, 3 h, 62% from **18**; (e) TBSOTf, 2,6-lutidine, CH_2Cl_2, 0 °C, 1 h, 98%; (f) DIBAL, CH_2Cl_2, −78 °C, 5 min; (g) $Ph_3P{=}CHCO_2Et$ (**10**), toluene, 110 °C, 3 h, 83% from **19**.

in **15** by reduction with lithium aluminum hydride and the successive oxidation of the primary alcohol **18** using tetrapropylammonium perruthenate (TPAP) afforded the (*E*,*E*)-dienealdehyde **12** in good yield. The enantioselective Mukaiyama aldol reaction[10] of **12** with KSA **13** in the presence of the chiral Sn(II) complex **14** smoothly took place to exclusively provide the desired *α*,*β*,*γ*-trisubstituted thioester **11**. Protection of the free hydroxyl group in **11** and reduction of the resulting *tert*-butyldimethylsiloxy (TBS) ether **19** with diisobutylaluminum hydride (DIBAL) were carried out to afford the chiral aldehyde **9**, and then the sequential treatment of **9** with Wittig reagent

dx.doi.org/10.1021/jm301695c | J. Med. Chem. 2013, 56, 150–159

10 afforded the α,β-unsaturated ester **8** as the key synthetic intermediate.

Before attempting the formation of the main skeleton of **1** from **8** by the IMDA reaction, we investigated the computer-aided prediction of the preferable stereoselectivity through theoretical calculations of the stability of the transition structures[14,15] using a simplified model compound **8M**, in which the TBSO group of **8** was replaced with a MeO group (Scheme 3).

Scheme 3. Predicted Preference of Diastereoselectivity in the IMDA Reaction of the Model Compound 8M Based on DFT Calculations

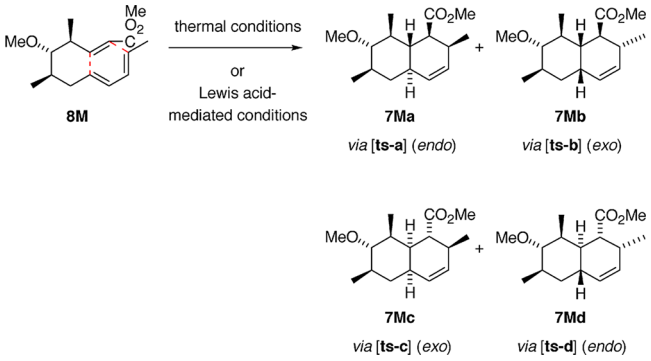

DFT calculations were performed to determine the transition structures that form the fused bicyclic backbone of the multisubstituted 3,4,4a,5,6,7,8,8a-octahydronaphthalene ($\Delta^{1,2}$-octalin). The geometries of all the stationary points were fully optimized at the B3LYP/6-31G* level of theory, and the properties of the molecules were also calculated at the same or advanced level using 6-31G**, 6-311G*, and 6-311G** basis functions. All points were characterized as minima or saddle points by calculation of the harmonic vibrational frequencies using analytical second derivatives.[16]

Four transition states provide the [4 + 2] cycloadducts **7Ma–d**, and these transition structures ([**ts-a1**]–[**ts-d1**]) are categorized as *endo*- and *exo*-modes (*endo*, [**ts-a1**] and [**ts-d1**]; *exo*, [**ts-b1**] and [**ts-c1**]) as depicted in Scheme 4 and Figure 2.

Scheme 4. Transition Structures of the Thermal IMDA Reaction of 8M

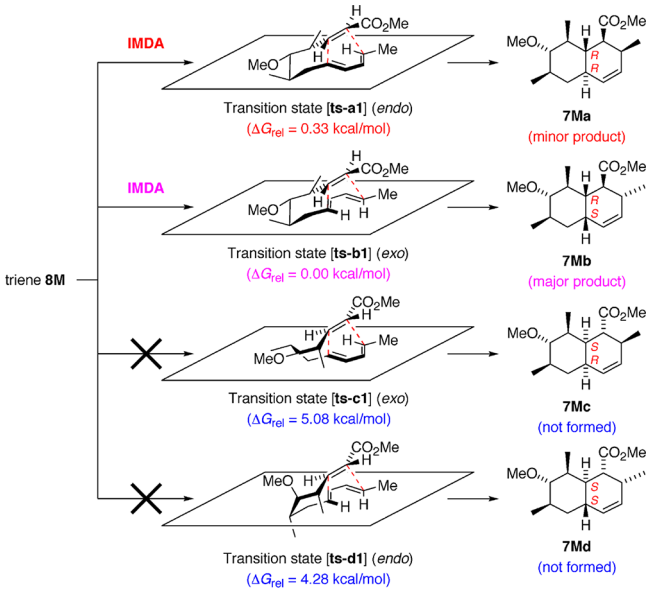

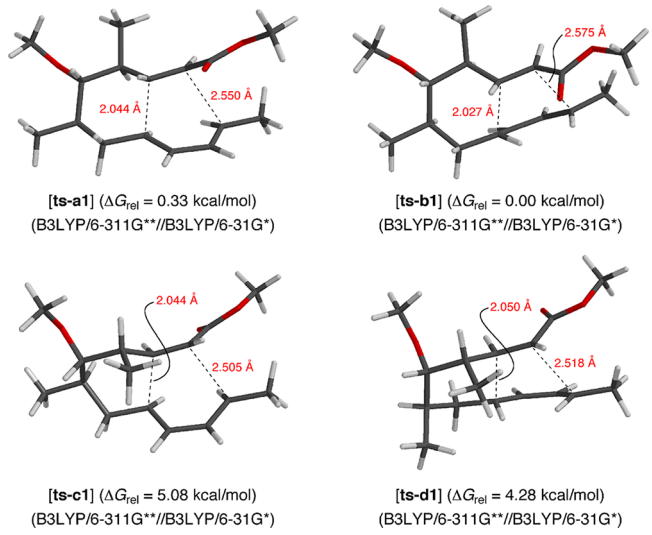

Figure 2. Three-dimensional transition structures, [**ts-a1**] (*endo*), [**ts-b1**] (*exo*), [**ts-c1**] (*exo*), and [**ts-d1**] (*endo*), in the thermal IMDA reaction of **8M**.

Table 1. Calculated Relative Gibbs Free Energies (ΔG_{rel}) (in kcal/mol) of the Transition Structures in the Thermal IMDA Reaction of 8M

	B3LYP/ 6-31G*	B3LYP/ 6-31G**	B3LYP/ 6-311G*	B3LYP/ 6-311G**	predict (110 °C)	
[**ts-a1**]	0.49 (0.40)[a]	0.50	0.19 (0.14)[a]	0.33	37 ..	45 ..
[**ts-b1**]	0.00 (0.00)[a]	0.00	0.00 (0.00)[a]	0.00	63 ..	~ 55 ..
[**ts-c1**]	5.21 (5.12)[a]	5.19	5.26 (5.23)[a]	5.08	0 ..	0 ..
[**ts-d1**]	4.65 (4.64)[a]	4.62	4.39 (4.48)[a]	4.28	0	0

[a]The values in parentheses are ΔG_{rel} values at 383.15 K (110 °C).

Scheme 5. Thermal or Et_2AlCl-Mediated IMDA Reaction of 8 to Form *endo*-Type (9*R*,10*R*)-$\Delta^{1,2}$-Octalin 20a via 7a and *exo*-Type (9*S*,10*R*)-$\Delta^{1,2}$-Octalin 20b via 7b[a]

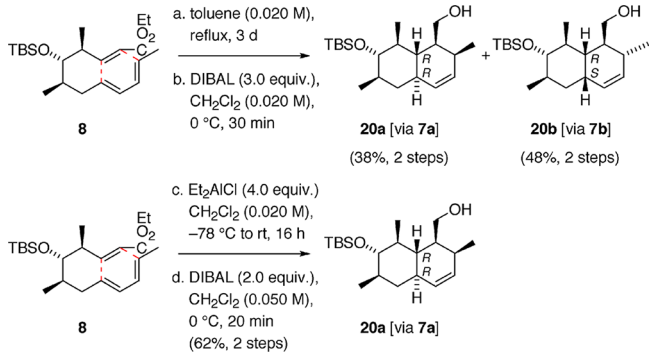

[a]Reagents and conditions: (a) toluene, reflux, 3 d; (b) DIBAL, CH_2Cl_2, 0 °C, 30 min, 38% of **20a** and 48% of **20b** from **8**; (c) Et_2AlCl, CH_2Cl_2, −78 °C to rt, 16 h; (d) DIBAL, CH_2Cl_2, 0 °C, 20 min, 62% of **20a** from **8**.

The desired (9*R*,10*R*)-$\Delta^{1,2}$-octalin derivative **7Ma** could be generated via the transition state [**ts-a1**] by the IMDA reaction of the model triene **8M**. Another *endo*-mode transition state [**ts-d1**] to form the diastereoisomeric (9*S*,10*S*)-$\Delta^{1,2}$-octalin derivative **7Md** is an unfavorable structure for the preparation of **1**. Similarly, the *exo*-mode transition states, [**ts-b1**] and [**ts-c1**], could be converted into the undesired (9*S*,10*R*)- and (9*R*,10*S*)-$\Delta^{1,2}$-octalin

dx.doi.org/10.1021/jm301695c | J. Med. Chem. 2013, 56, 150–159

Scheme 6. Transition Structures of the Me_2AlCl-Mediated IMDA Reaction of 8M

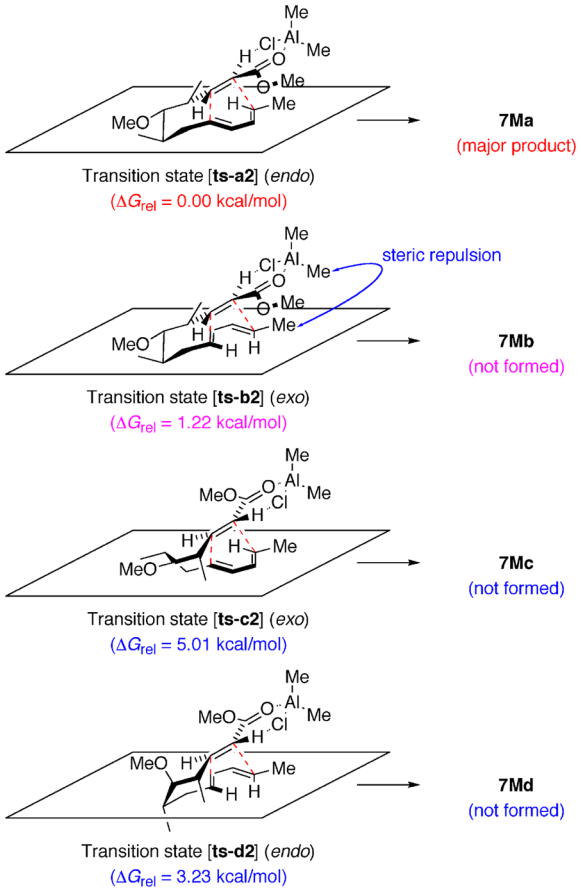

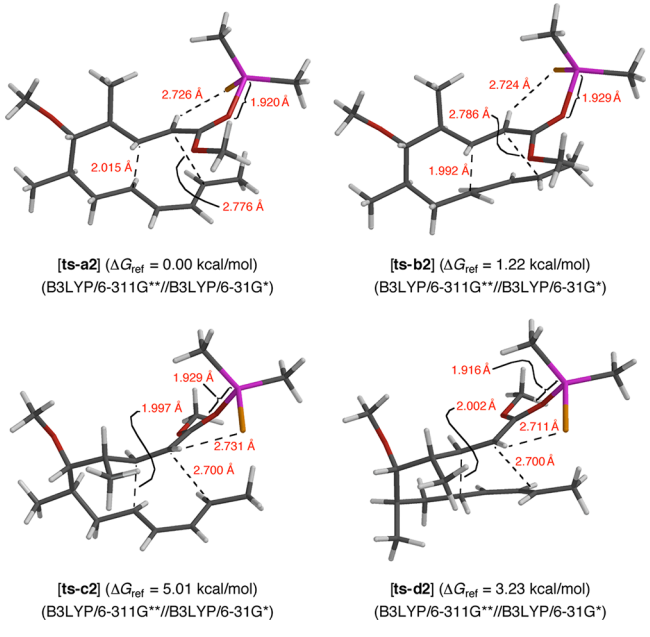

Figure 3. Three-dimensional transition structures, [**ts-a2**] (*endo*), [**ts-b2**] (*exo*), [**ts-c2**] (*exo*), and [**ts-d2**] (*endo*), in the Me_2AlCl-mediated IMDA reaction of **8M**.

derivatives **7Mb** and **7Mc** through the imaginary IMDA reactions, respectively. The calculated relative Gibbs free energy (ΔG_{rel}) is shown under each transition structure in Scheme 4 and Table 1. It was revealed that [**ts-c1**] and [**ts-d1**] have significantly high ΔG_{rel} values compared with those of [**ts-a1**] and [**ts-b1**] because of the steric repulsion between the methyl group at the C-4 position in **8M** and the surroundings in these transition structures. Therefore, the corresponding (9*R*,10*S*)- and (9*S*,10*S*)-$\Delta^{1,2}$-octalin derivatives **7Mc** and **7Md** will hardly form via these two highly strained transition states (ΔG_{rel} = 5.21−5.08 kcal/mol for [**ts-c1**]; ΔG_{rel} = 4.65−4.28 kcal/mol for [**ts-d1**]). Within the stable [**ts-a1**] and [**ts-b1**] structures having lower values of ΔG_{rel}, the formation of the latter transition structure is preferable. The calculated free-energy

Table 2. Calculated Relative Gibbs Free Energies (ΔG_{rel}) (in kcal/mol) of the Transition Structures in the Me_2AlCl-Mediated IMDA Reaction of 8M

	B3LYP/ 6-31G*	B3LYP/ 6-31G**	B3LYP/ 6-311G*	B3LYP/ 6-311G**	predict (25 °C)
[**ts-a2**]	0.00	0.00	0.00	0.00	93 .. 89
[**ts-b2**]	1.50	1.41	1.32	1.22	7 .. ∼ .. 11
[**ts-c2**]	5.33	5.27	5.23	5.01	0 .. 0
[**ts-d2**]	3.48	3.34	3.51	3.23	0 0

Scheme 7. Completion of Total Syntheses of 1 and 2[a]

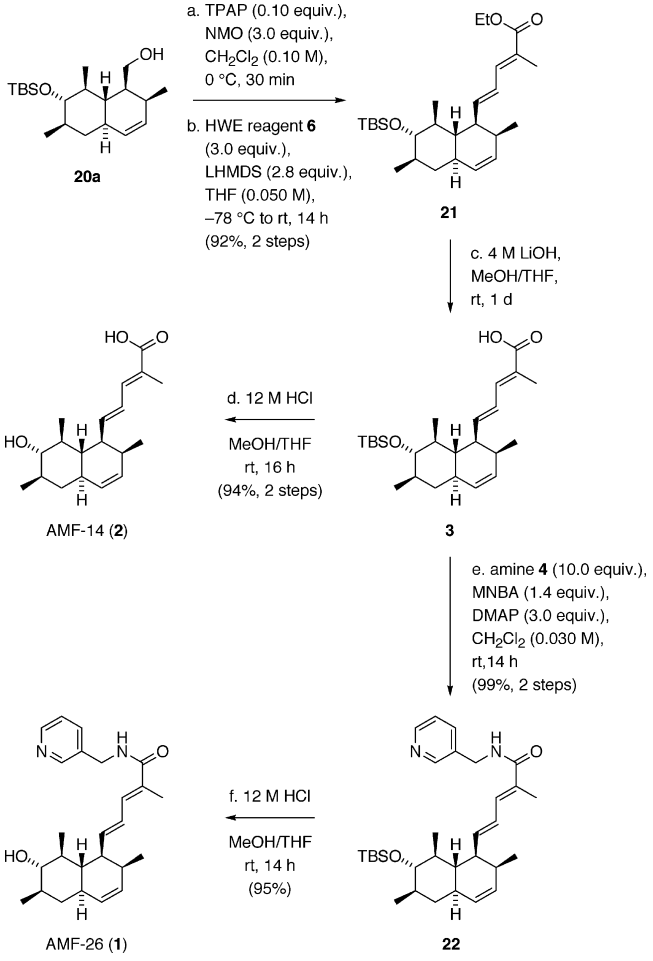

[a]Reagents and conditions: (a) TPAP, NMO, CH_2Cl_2, 0 °C, 30 min; (b) phosphate **6**, LHMDS, THF, −78 °C to rt, 14 h, 92% from **20a**; (c) 4 M LiOH, MeOH, THF, rt, 1 d; (d) 12 M HCl, MeOH, THF, rt, 16 h, 94% from **21**; (e) amine **4**, MNBA, DMAP, CH_2Cl_2, rt, 14 h, 99% from **21**; (f) 12 M HCl, MeOH, THF, rt, 14 h, 95%.

dx.doi.org/10.1021/jm301695c | J. Med. Chem. 2013, 56, 150−159

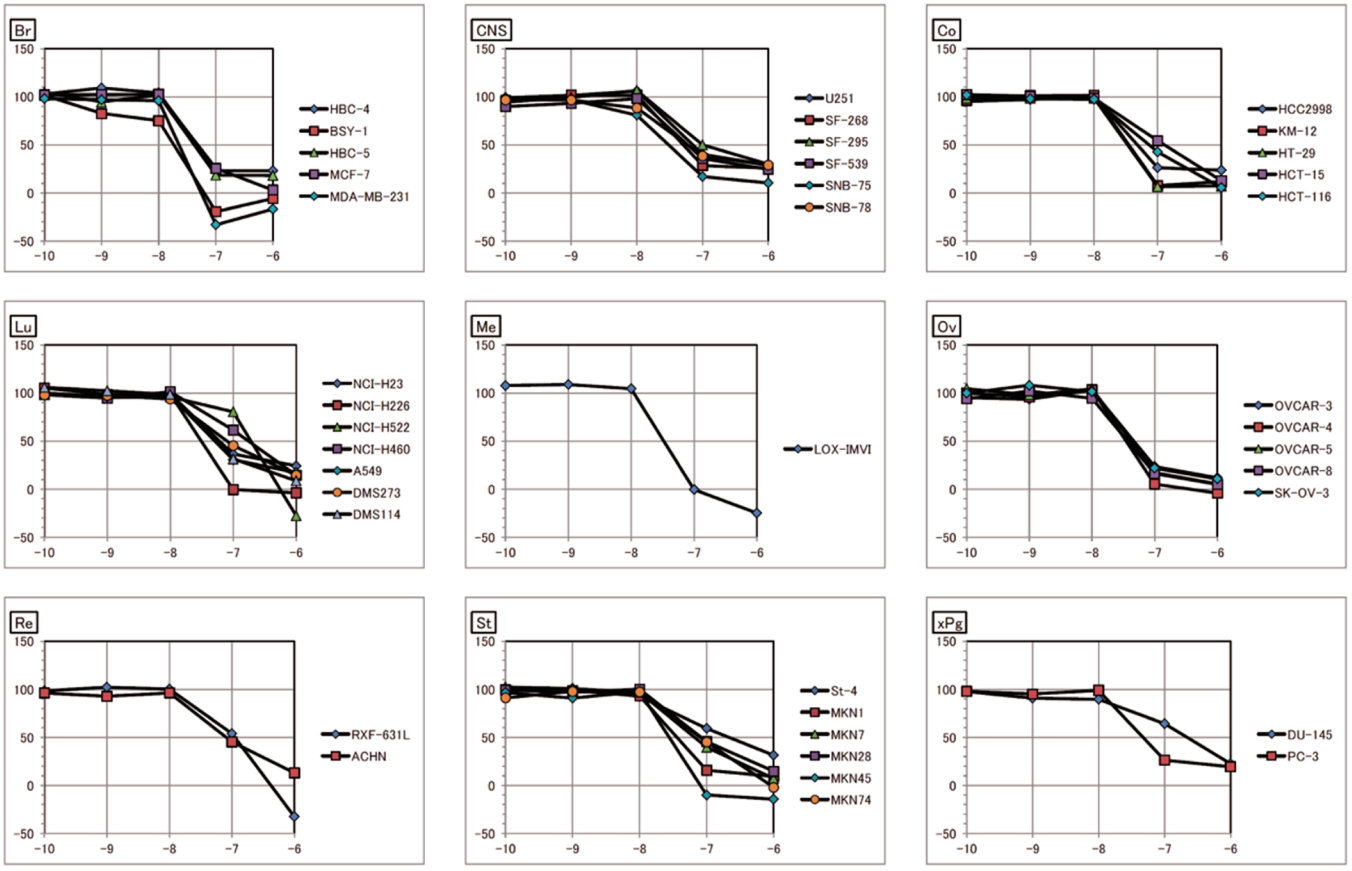

Figure 4. Growth inhibition against a panel of human cancer cell lines. Dose-dependent effects of the totally synthetic **1** on each cancer cell were measured as described in the experimental procedures. The *x*-axis represents the logarithm of the mean of the GI50 values (log[concentration (M)]) for each cell line. The *y*-axis represents the growth rate of each human cancer cell line (% of control). Quantification of the GI50 value was represented as the mean of four different experiments. Br, breast; CNS, central nervous system; Co, colon; Lu, lung; Me, melanoma; Ov, ovary; Re, renal; St, stomach; xPg, prostate.

difference (ΔG_{rel} = 0.49−0.19 kcal/mol at 298.15 K (25 °C); 0.40−0.14 kcal/mol at 383.15 K (110 °C)) corresponds to the medium diastereomeric ratio of the formed [4 + 2] cycloadducts according to the Boltzmann distribution (estimated selectivity of **7Ma**:**7Mb** = ∼30:70−42:58 at 298.15 K (25 °C); ∼37:63−45:55 at 383.15 K (110 °C)).

Thermal IMDA Reaction of 8 to Form $\Delta^{1,2}$-Octalins 20a and 20b and Et_2AlCl-Mediated Diastereoselective IMDA Reaction of 8 to Form $\Delta^{1,2}$-Octalin 20a. After determining the transition structures and understanding the nature of the predictable stereoselectivity of the IMDA reaction of **8M**, we eventually examined the thermal transformation of **8**, which has a TBSO group at the C-5 position instead of a MeO group at the same position in **8M**. By heating **8** in toluene at reflux temperature for three days (Scheme 5, upper equation), the desired thermal [4 + 2] cycloaddition reaction successfully proceeded, and we obtained a mixture of two stereoisomeric products, **7a** and **7b**, corresponding to the model $\Delta^{1,2}$-octalins **7Ma** and **7Mb**, respectively. A mixture of the cycloadducts, **7a** and **7b**, was then treated with DIBAL to provide the desired primary alcohols, **20a** and **20b**, with a low diastereoselectivity (**20a**:**20b** = ∼44:56) in this two-step transformation. These experimental results are in good agreement with the assumed stereoselectivity as follows: (1) Two products, **7a** and **7b**, possessing (*R*) configurations at the C-10 position were predominantly produced, and two other $\Delta^{1,2}$-octalins possessing (*S*) configurations at the same position were not obtained at all. (2) Both the major stereoisomer, (9*S*,10*R*)-**7b**, generated from the *exo*-mode transition state, and the minor one, (9*R*,10*R*)-**7a**, generated from the *endo*-mode transition state, were simultaneously produced because the predicted preference of the *exo*-mode transition state over the *endo*-mode transition state is not very high.

To improve the yield of the *endo*-type (9*R*,10*R*)-$\Delta^{1,2}$-octalin derivative **7a**, a favorable intermediate for the synthesis of **1**, it is necessary to develop an alternative activation method for the IMDA reaction that proceeds via the *endo*-mode transition state [**ts-a1**] but not via the *exo*-mode transition state [**ts-b1**]. There are many successful examples of obtaining *endo*-type octalin derivatives via the diastereoselective Diels−Alder reaction using a Lewis acid in steroid syntheses;[17] therefore, we decided to use the Et_2AlCl-mediated Diels−Alder reaction to control the diastereoselectivity of the IMDA reaction of **8**.

Determination of the structures of the *endo*- and *exo*-mode transition states with Me_2AlCl and the relative Gibbs free energies was next carried out by theoretical calculations according to the above-mentioned method for predicting the diastereoselectivity that uses the model substrate **8M**. The optimized *endo*-mode transition structures [**ts-a2**] and [**ts-d2**], and *exo*-mode transition structures [**ts-b2**] and [**ts-c2**] are described in Scheme 6 and Figure 3, in which all ester-carbonyl groups are activated by Me_2AlCl. Each chloride atom in [**ts-a2**]−[**ts-d2**] locates near an α-proton of the ester group because a hydrogen-bonding interaction occurs between the electronically negative chloride atom and electronically positive hydrogen atom. Therefore, stable

dx.doi.org/10.1021/jm301695c | *J. Med. Chem.* 2013, 56, 150−159

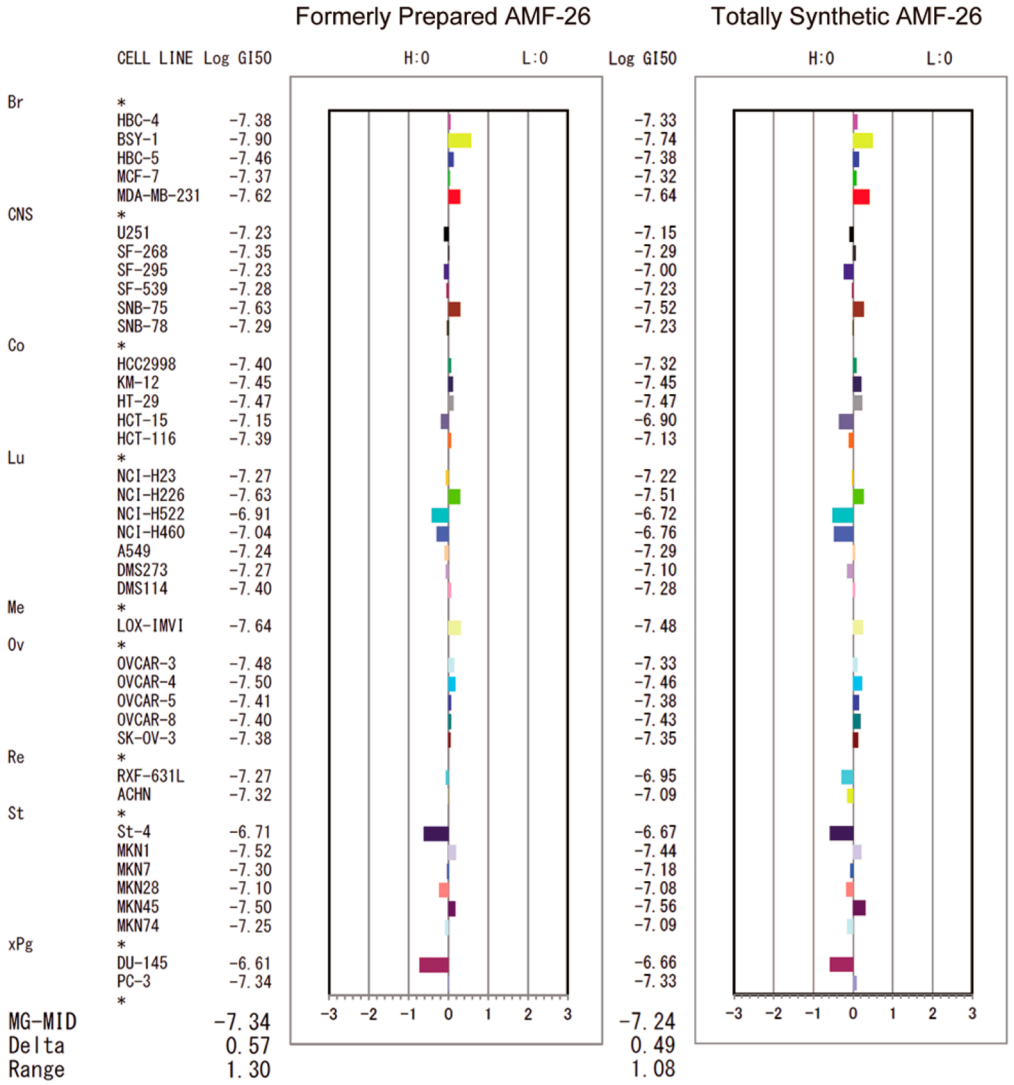

Figure 5. Fingerprints of the formerly prepared **1** and totally synthetic **1**. Growth inhibition was assessed against a panel of 39 human cancer cell lines. Fingerprints were produced by computer processing of the 50% growth inhibition (GI50) values. The logarithm of the GI50 value for each cell line is indicated in the figure. In the plot, columns to the right of zero indicate the sensitivity of the cell line to the compound, and columns to the left indicate resistance to the compound. The *x*-axis represents the logarithm of the difference between the mean of the GI50 values for 39 cell lines and the GI50 value for each cell line in the JFCR39 panel. The fingerprint of the totally synthetic **1** (right column) significantly correlated with that of the formerly prepared **1** derived from a natural molecule **2** (left column) (Pearson correlation coefficient $r = 0.843$). MG-MID, the mean of the log GI50 values for the 39 cell lines; delta, the logarithm of the difference between the MG-MID and log GI50 of the most sensitive cell line; range, the logarithm of the difference between the log GI50 of the most resistant cell line and log GI50 of the most sensitive cell line. One scale represents one logarithm difference.

six-membered rings, including (i) a strong coordination of the oxygen atoms in ester groups to aluminum atoms and (ii) an additional hydrogen-bonding interaction between the chloride atoms in Me_2AlCl and C-2 protons of the ester groups, were efficiently created in these transition states. However, the calculated relative Gibbs free energies in Table 2 indicate that (i) [**ts-c2**] and [**ts-d2**] have higher ΔG_{rel} values (5.33−5.01 kcal/mol for [**ts-c2**]; 3.51−3.23 kcal/mol for [**ts-d2**]) compared with those of [**ts-a2**] and [**ts-b2**] similar to the thermal IMDA reaction of **8M**, (ii) the *endo*-mode transition state [**ts-a2**] is more stable than the *exo*-mode transition state [**ts-b2**] because the ΔG_{rel} of [**ts-a2**] is much lower than that of [**ts-b2**] (ΔG_{rel} = 1.50−1.22 kcal/mol at 298.15 K (25 °C)). It is assumed that the steric repulsion between one of the methyl groups in Me_2AlCl and the substrate is quite high during the conversion of the triene **8M**−Me_2AlCl complex into the transition structure [**ts-b2**] as depicted in Scheme 6.

On the basis of the present preferable theoretical prediction, we actually examined the IMDA reaction of **8** using Et_2AlCl instead of the ideal reaction of **8M** with Me_2AlCl, and the desired **20a** was solely obtained after reducing the temporarily formed **7a**; namely, the production of the *endo*-type (9*R*,10*R*)-$\Delta^{1,2}$-octalin derivative **7a** exclusively occurs without formation of not only the *exo*-type (9*S*,10*R*)-$\Delta^{1,2}$-octalin derivative **7b** but also other stereoisomers, such as the (9*R*,10*S*)- and (9*S*,10*S*)-$\Delta^{1,2}$-octalin derivatives **7c** and **7d** (Scheme 5, bottom equation).

Completion of the First Total Synthesis. Next, installation of the $\alpha,\beta,\gamma,\delta$-bisunsaturated ester moiety in the (9*R*,10*R*)-$\Delta^{1,2}$-octalin derivative **20a** was attempted, as shown in Scheme 7. Oxidation of **20a** using TPAP with NMO was carried out to provide the corresponding aldehyde **5**, and the following HWE olefination of the resulting aldehyde **5** with phosphate **6**[18] smoothly proceeded to afford the desired triene **21** in good yield. After hydrolysis of the ester moiety in **21** with lithium hydroxide,

dx.doi.org/10.1021/jm301695c | J. Med. Chem. 2013, 56, 150−159

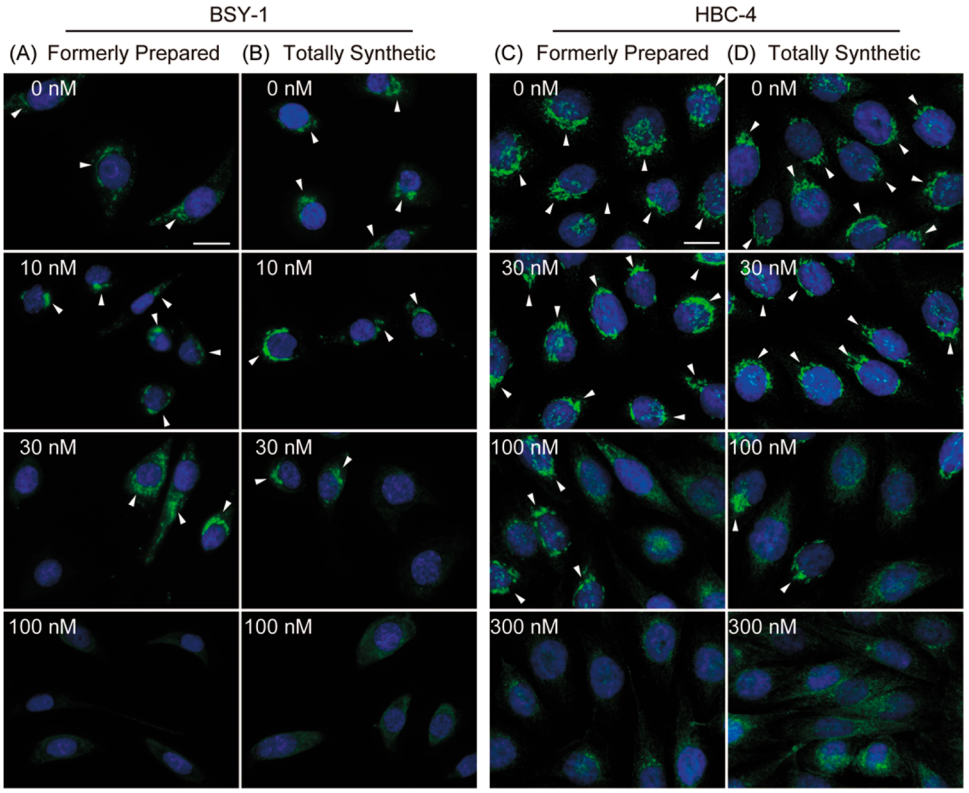

Figure 6. Disrupting Golgi apparatus by the formerly prepared **1** and totally synthetic **1** [dispersion of GBF1 in BSY-1 cells (A and B) or HBC-4 cells (C and D)]. Cells were treated with either the formerly prepared **1** (A and C) or the totally synthetic **1** (B and D) at different concentrations for 1 h. The cells were then fixed and labeled with anti GBF1 (green) and DAPI (blue). In the BSY-1 and HBC-4 cells treated with the formerly prepared **1** or the totally synthetic **1**, GBF1 was dispersed from the perinuclear region, which gave a ribbon-like appearance (white arrowhead), into the cytoplasm. Scale bar: 20 μm.

deprotection of the silyl ether group at the C-6 position of the resulting carboxylic acid **3** was eventually examined using 12 M hydrochloric acid, and the desired product **2** was readily prepared in excellent yield by this facile procedure.[19] All the spectral data, including the optical rotation of the totally synthetic **2**, corresponded to those reported for naturally occurring (+)-**2** (our synthetic sample; $[\alpha]_D^{24}$ +56.4 (*c* 0.593, MeOH), lit[1,2] $[\alpha]_D^{20}$ +58.71 (*c* 0.998, MeOH)), and all the absolute configurations of the stereogenic centers at the C-3, C-4, C-5, C-6, C-7, C-9, and C-10 positions were unequivocally determined by this identification. On the other hand, it was revealed that MNBA-mediated amidation[12] using an excess amount of DMAP (3.0 equiv) in the absence of triethylamine produced the 3-picolylamide **22** from the carboxylic acid **3** in a satisfactory yield. Finally, the transformation of **22** by deprotection of the TBS group furnished the targeted molecule **1** in very high yield.[19] Thus, an efficient method for the synthesis of **1** was established via the Et_2AlCl-mediated diastereoselective IMDA reaction of the chiral linear precursor **8**. The synthesis of **1** proceeds in 14 steps and 19% overall yield from the chiral oxazolidinone **16**. The ^1H and ^{13}C NMR spectra of the obtained **1** showed that the synthetic sample has the same relative stereochemistry as formerly prepared **1** derived from naturally occurring **2**. Other properties of the synthetic **1** including its optical rotation were identical to those of formerly prepared (+)-**1** derived from (+)-**2** (our synthetic sample; $[\alpha]_D^{26}$ +73.6 (*c* 0.480, MeOH), lit[1,2] $[\alpha]_D^{20}$ +76.69 (*c* 1.103, MeOH)).

BIOLOGICAL ASSAYS OF THE TOTALLY SYNTHETIC AMF-26

Antitumor Activity of the Totally Synthetic 1 against a Variety of Human Cancer Cell Lines. To obtain a preliminary evaluation of the totally synthetic **1**, we determined the biological activity of the synthetic **1** for cell growth inhibition and disrupting the Golgi system. As shown in Figure 4, the global antitumor activity of the totally synthetic **1** against a variety of human cancer cells was assessed on a panel of 39 human cancer cell lines (JFCR39).[2,20] Among them, the synthetic **1** strongly inhibited the growth of several cancer cell lines at concentrations of less than 0.04 μM (GI50 values at 18.2 nM for BSY-1, 22.9 nM for MDA-MB-231 [breast], 30.2 nM for SNB-75 [central nervous system], 35.5 nM for KM-12, 33.9 nM for HT-29 [colon], 30.9 nM for NCI-H226 [lung], 33.1 nM for LOX-IMVI [melanoma], 34.7 nM for OVCAR-4, 37.2 nM for OVCAR-8 [ovary], and 36.3 nM for MKN1, 27.5 nM for MKN45 [stomach]).

The informatic anticancer drug discovery system, JFCR39, is a powerful tool for extracting compounds with similar modes of action from a database.[20] The JFCR39 panel was coupled with our own drug sensitivity database, which is comparable to that of the NCI60 panel from the National Cancer Institute.[21] By using the COMPARE computer algorithm (details described in the experimental procedures), it is possible to correlate the growth inhibitory patterns of JFCR39 (termed "fingerprints") of a test compound with those of a known compound in the database. We compared the fingerprint of the totally synthetic **1** with that of the formerly prepared **1** derived from a natural molecule **2** (Figure 5) and demonstrated a significant correlation between the two (correlation coefficient r = 0.843).

Golgi Disruption and Proliferation Tests of BSY-1 and HBC-4 Cells by the Totally Synthetic AMF-26. We previously reported that **1** disrupted the Golgi system by inhibiting the Arf1 activation.[2] We now examined whether the totally synthetic **1** induced Golgi disassembly by use of immunofluorescence

dx.doi.org/10.1021/jm301695c | J. Med. Chem. 2013, 56, 150−159

staining with a monoclonal antibody to GBF1 (Golgi brefeldin A resistant guanine nucleotide exchange factor 1), a marker of Golgi. In the control cells, GBF1 was observed in the perinuclear region. The addition of the totally synthetic **1** caused a rapid release of GBF1 into the cytoplasm as shown in parts B and D of Figure 6, similar to the addition of the formerly prepared **1** derived from a natural molecule **2**, as shown in parts A and C of Figure 6.

The proliferation of BSY-1 or HBC-4 cells treated with drugs was monitored as shown in Figure 7A. Changes in the amounts of the total cellular protein after 48 h of drug treatment were analyzed using the SRB assay. Furthermore, the BSY-1 or HBC-4 cells were treated with the formerly prepared **1** and totally synthetic **1** at different concentrations for 1 h and then stained with antibodies against GBF1 (Figure 7B). Over 100 features were measured under each condition, and the numbers of cells whose Golgi was dispersed were then counted. The biological efficacy of the totally synthetic **1** was consistent with that of the semisynthesized **1** based on these data; therefore, we concluded that the structure of the totally synthetic **1** was unambiguously identified with that of the formerly prepared **1**, which was derived from a natural compound **2**.

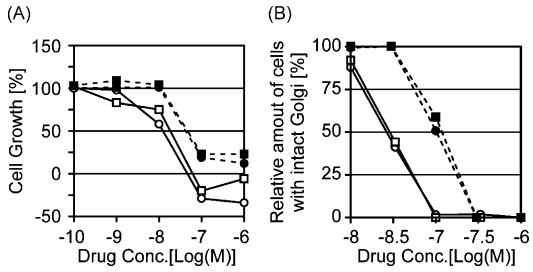

Figure 7. Cell growth inhibition and Golgi disruption by the formerly prepared **1** and totally synthetic **1**. Symbols represent the following: open circle, BSY-1 cells treated with the formerly prepared **1**; open square, BSY-1 cells treated with the totally synthetic **1**; closed circle, HBC-4 cells treated with the formerly prepared **1**; closed square, HBC-4 cells treated with the totally synthetic **1**.

SYNTHESIS AND SAR STUDIES OF AMF-26 DERIVATIVES

By use of intermediate **20a**, we further prepared compounds **26** and **31** as derivatives of **1** as depicted in Schemes 8 and 9, respectively. The two-carbon elongation of the aldehyde derived from **20a** was carried out to afford the corresponding unsaturated ester **23** (Scheme 8). The saponification of **23** and the successive MNBA-mediated amidation of **24** provided **25** in a very high yield. Finally, compound **26**, which includes a shortened side-chain compared to **1**, was successfully obtained by the treatment of **25** with hydrochloric acid. We also prepared another derivative **31** according to the procedure for the synthesis of **1**. As depicted in Scheme 9, compound **31** has a longer alkyl group (ethyl group) at the α-position of the amide group instead of a methyl group at the same position in **1**. We then tried to evaluate the efficacy of these novel derivatives, **26** and **31**, based on SAR studies of the side-chain in **1**. We first determined the biological activity of these derivatives for cell growth inhibition using JFCR39. Figure 1 in the Supporting Information represents fingerprints of the formerly prepared **1**, the totally synthetic **1**, compound **26**, and compound **31**. The experimental conditions and abbreviations are described in Figure 5. The logarithm of the mean GI50 values of compound **31** was −6.11, meaning that the

Scheme 8. Preparation of a Novel Derivative 26[a]

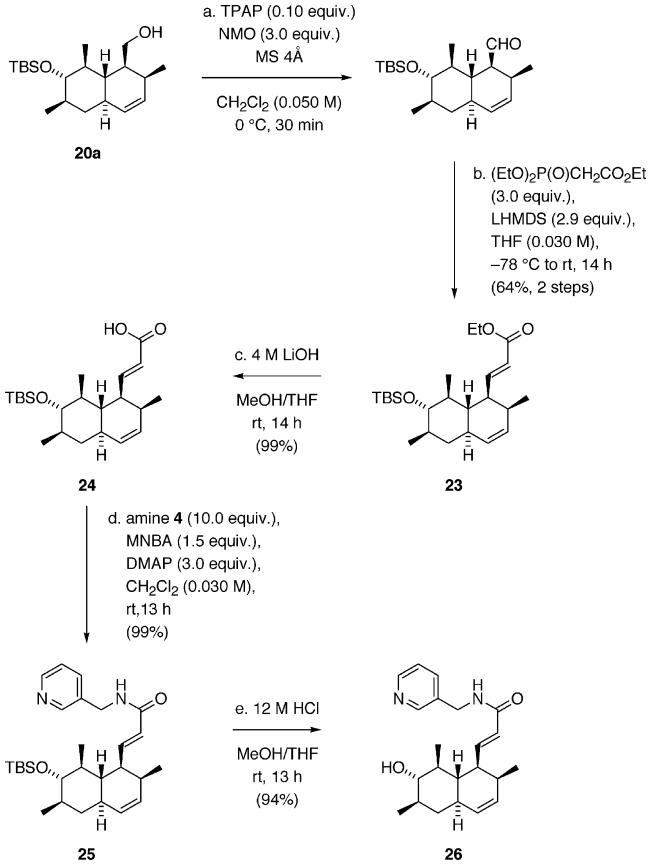

[a]Reagents and conditions: (a) TPAP, NMO, 4-Å molecular sieves, CH_2Cl_2, 0 °C, 30 min; (b) $(EtO)_2P(O)CH_2CO_2Et$, LHMDS, THF, −78 °C to rt, 14 h, 64% from **20a**; (c) 4 M LiOH, MeOH, THF, rt, 14 h, 99%; (d) amine **4**, MNBA, DMAP, CH_2Cl_2, rt, 13 h, 99%; (e) 12 M HCl, MeOH, THF, rt, 13 h, 94%.

growth inhibition efficacy of compound **31** was about 10-fold weaker than that of **1** and its efficacy of the growth inhibition was moderate. The fingerprint of compound **31** significantly correlated that of the formerly prepared **1** (correlation coefficient $r = 0.816$). On the other hand, the logarithm of the mean GI50 values of compound **26** was −4.02, suggesting that this compound showed a very weak efficacy. There was no correlation between the fingerprint of compound **26** and that of the formerly prepared **1** ($r = 0.117$).

Next, we examined the Golgi disruption efficacy of the two derivatives. The addition of compound **31** caused a release of GBF1 into the cytoplasm as depicted in parts B and D of Figure 2 in the Supporting Information. However, no Golgi disruption was observed at the concentration of 1 μM in the compound-**26**-treated BSY-1 cells as depicted in Figure 2A of the Supporting Information or 10 μM in the compound-**26**-treated HBC-4 cells as depicted in Figure 2C of the Supporting Information.

The proliferation of BSY-1 or HBC-4 cells treated with drugs (formerly prepared **1**, the totally synthetic **1**, compound **26**, and compound **31**) was monitored as shown in parts A and B of Figure 3 in the Supporting Information. Furthermore, the observed Golgi disrupting efficacy of all drugs was shown in parts C and D of Figure 3 in the Supporting Information. Modification of the side-chain induced a wide range of biological efficacies. Compound **31** moderately inhibited cell growth (GI50 value at 0.55 μM for HBC-4 and 0.19 μM for BSY-1) and disrupted the Golgi

dx.doi.org/10.1021/jm301695c | J. Med. Chem. 2013, 56, 150−159

Scheme 9. Preparation of a Novel Derivative 31[a]

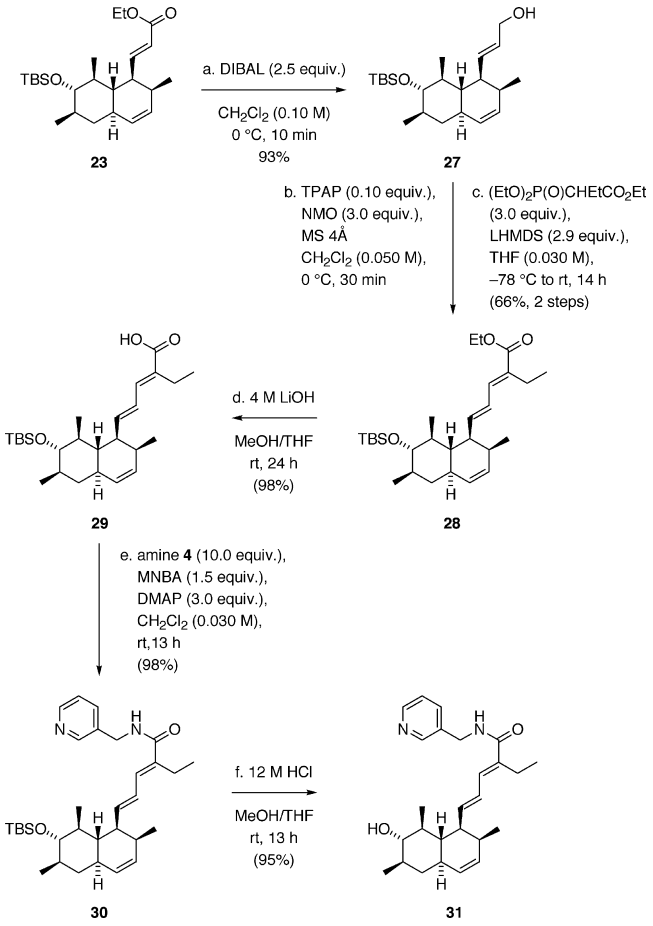

[a]Reagents and conditions: (a) DIBAL, CH_2Cl_2, 0 °C, 10 min, 93%; (b) TPAP, NMO, 4-Å molecular sieves, CH_2Cl_2, 0 °C, 30 min; (c) $(EtO)_2P(O)CHEtCO_2Et$, LHMDS, THF, −78 °C to rt, 14 h, 66% from **27**; (d) 4 M LiOH, MeOH, THF, rt, 24 h, 98%; (e) amine **4**, MNBA, DMAP, CH_2Cl_2, rt, 13 h; 98%; (f) 12 M HCl, MeOH, THF, rt, 13 h, 95%.

apparatus (EC50 value at 0.85 μM for HBC-4 and 0.34 μM for BSY-1); however, compound **26** showed very weak biological activities (both the GI50 value and EC50 value were above 10 μM).[22]

CONCLUSION

In summary, we have developed a convenient method for preparing **1**, a potentially promising new anticancer drug that disrupts the Golgi system by inhibiting the Arf1 activation. We achieved this total synthesis through the stereoselective IMDA reaction of the chiral linear precursor using Et_2AlCl as a Lewis-acid activator. The stereoselectivity of the thermal or Me_2AlCl-mediated IMDA reaction was theoretically presumed by DFT calculations, and the origins of the switching in the reaction modes under these two conditions were plausibly accounted for by a comparison between the relative Gibbs free energies of those transition states in the IMDA reaction. From an assessment of the global antitumor activity of the totally synthetic **1** against a variety of human cancer cells using a panel of 39 human cancer cell lines, it was shown that the synthetic **1** strongly inhibited the growth of several cancer cell lines, such as BSY-1, MDA-MB-231, SNB-75, KM-12, HT-29, NCI-H226, LOX-IMVI, OVCAR-4, OVCAR-8, MKN1, and MKN45, at low concentrations (less than 0.04 μM for GI50). An evaluation of the biological activities of the synthetic **1** in two types of assessments revealed that our synthetic **1** has the same property as the semisynthesized **1** derived from the original natural molecule **2** (correlation coefficient $r = 0.843$). Through both the total synthesis of **1** and identification of the synthetic **1** with the formerly prepared **1** regarding their biological activity, the structure of the formerly prepared **1** has been unequivocally determined. We further synthesized compound **26**, which includes a shortened side-chain compared to **1**, and another derivative **31**, which has a longer alkyl group at the α-position of the amide group instead of a methyl group at the same position in **1**. Compound **26** showed a very weak efficacy, and there was no correlation between the fingerprint of compound **26** and that of **1** ($r = 0.117$). On the other hand, the growth inhibition efficacy of compound **31** was about 10-fold weaker than that of **1** and its fingerprint was significantly correlated to that of **1** ($r = 0.816$). The large-scale production of **1** and its derivatives for the development of novel anticancer drugs are now in progress in this laboratory.

ASSOCIATED CONTENT

Supporting Information

Experimental procedures; supplementary figures for the SAR studies of AMF-26 derivatives **26** and **31**; spectroscopic and analytical data for all new compounds including copies of NMR spectra; Cartesian coordinates of transition states. This material is available free of charge via the Internet at http://pubs.acs.org.

AUTHOR INFORMATION

Corresponding Author

*Phone: +81-3-3260-4271. Fax: +81-3-3260-5609. E-mail: shiina@rs.kagu.tus.ac.jp.

Notes

The authors declare no competing financial interest.

ACKNOWLEDGMENTS

This study was supported by a Health and Labour Sciences Research Grants from the Ministry of Health, Labour and Welfare, Japan.

ABBREVIATIONS USED

ADP, adenosine diphosphate; Arf1, ADP-ribosylation factor 1; IMDA, intramolecular Diels−Alder; JFCR39, a panel of 39 human cancer cell lines in Japanese Foundation for Cancer Research; ArfGEF, guanine nucleotide exchange factor for Arf; VEGF, vascular endothelial growth factor; GBF1, Golgi brefeldin A resistant guanine nucleotide exchange factor 1; DAPI, 4′,6-diamidino-2-phenylindole; KSA, ketene silyl acetal; HWE, Horner−Wadsworth−Emmons; MNBA, 2-methyl-6-nitrobenzoic anhydride; DMAP, 4-(dimethylamino)pyridine; NaHMDS, sodium bis(trimethylsilyl)amide; LHMDS, lithium bis(trimethylsilyl)-amide; TBAI, tetrabutylammonium iodide; TPAP, tetrapropylammonium perruthenate; NMO, 4-methylmorpholine *N*-oxide; TBS, *tert*-butyldimethylsiloxy; DIBAL, diisobutylaluminum hydride; DFT, density functional theory

REFERENCES

(1) Yamada, N. WO2005/070856, 2005, Nippon Shinyaku Co., Ltd.

(2) Ohashi, Y.; Iijima, H.; Yamaotsu, N.; Yamazaki, K.; Sato, S.; Okamura, M.; Sugimoto, K.; Dan, S.; Hirono, S.; Yamori, T. *J. Biol. Chem.* **2012**, *287*, 3885−3897.

(3) Reviews for drug discovery at protein−protein interfaces. (a) Berg, T. *Curr. Opin. Drug Discov. Dev.* **2008**, *11*, 666−674. (b) Wells, J. A.; McClendon, C. L. *Nature* **2007**, *450*, 1001−1009.

(4) Inhibition of Arf1−ArfGEF interaction by brefeldin A: (a) Renault, L.; Guibert, B.; Cherfils, J. *Nature* **2003**, *426*, 525−530. (b) Zeeh, J. C.; Zeghouf, M.; Grauffel, C.; Guibert, B.; Martin, E.; Dejaegere, A.; Cherfils, J. *J. Biol. Chem.* **2006**, *281*, 11805−11814.
(5) Disruption of the Golgi apparatus by brefeldin A: (a) Lippincott-Schwartz, J.; Yuan, L. C.; Bonifacino, J. S.; Klausner, R. D. *Cell* **1989**, *56*, 801−813. (b) Lippincott-Schwartz, J.; Yuan, L.; Tipper, C.; Amherdt, M.; Orci, L.; Klausner, R. D. *Cell* **1991**, *67*, 601−616.
(6) Inhibition of tumor growth by brefeldin A: (a) Sausville, E. A.; Duncan, K. L.; Senderowicz, A.; Plowman, J.; Randazzo, P. A.; Kahn, R.; Malspeis, L.; Grever, M. R. *Cancer J. Sci. Am.* **1996**, *2*, 52−58. (b) Häcki, J.; Egger, L.; Monney, L.; Conus, S.; Rossé, T.; Fellay, I.; Borner, C. *Oncogene* **2000**, *19*, 2286−2295.
(7) Anadu, N. O.; Davisson, V. J.; Cushman, M. *J. Med. Chem.* **2006**, *49*, 3897−3905.
(8) Watari, K.; Nakamura, M.; Fukunaga, Y.; Furuno, A.; Shibata, T.; Kawahara, A.; Hosoi, F.; Kuwano, T.; Kuwano, M.; Ono, M. *Int. J. Cancer* **2012**, *131*, 310−321.
(9) (a) Evans, D. A.; Ennis, M. D.; Mathre, D. J. *J. Am. Chem. Soc.* **1982**, *104*, 1737−1739. (b) Evans, D. A.; Bartroli, J. *Tetrahedron Lett.* **1982**, *23*, 807−810.
(10) (a) Mukaiyama, T.; Kobayashi, S.; Uchiro, H.; Shiina, I. *Chem. Lett.* **1990**, 129−132. (b) Kobayashi, S.; Uchiro, H.; Fujishita, Y.; Shiina, I.; Mukaiyama, T. *J. Am. Chem. Soc.* **1991**, *113*, 4247−4252. (c) Shiina, I. In *Modern Aldol Reactions*; Mahrwald, R., Eds.; Wiley-VCH: Weinheim, 2004, pp 105−165.
(11) Reviews for IMDA reaction for the synthesis of natural products. (a) Takao, K.; Munakata, R.; Tadano, K. *Chem. Rev.* **2005**, *105*, 4779−4807. (b) Juhl, M.; Tanner, D. *Chem. Soc. Rev.* **2009**, *38*, 2983−2992.
(12) (a) Shiina, I.; Kawakita, Y. *Tetrahedron* **2004**, *60*, 4729−4733. (b) Shiina, I.; Ushiyama, H.; Yamada, Y.; Kawakita, Y.; Nakata, K. *Chem. Asian J.* **2008**, *3*, 454−461. See also (c) Shiina, I.; Kubota, M.; Oshiumi, H.; Hashizume, M. *J. Org. Chem.* **2004**, *69*, 1822−1830. (d) Shiina, I.; Umezaki, Y.; Kuroda, N.; Iizumi, T.; Nagai, S.; Katoh, T. *J. Org. Chem.* **2012**, *77*, 4885−4901.
(13) (a) Sarpong, R.; Su, J. T.; Stoltz, B. M. *J. Am. Chem. Soc.* **2003**, *125*, 13624−13625. (b) Taber, D. F.; Guo, P.; Guo, N. *J. Am. Chem. Soc.* **2010**, *132*, 11179−11182. (c) Bross, H.; Schneider, R.; Hopf, H. *Tetrahedron Lett.* **1979**, *20*, 2129−2132.
(14) DFT study of the thermal and Lewis acid catalyzed Diels−Alder reaction: (a) Goldstein, E.; Beno, B.; Houk, K. N. *J. Am. Chem. Soc.* **1996**, *118*, 6036−6043. (b) García, J. I.; Martínez-Merino, V.; Mayoral, J. A.; Salvatella, L. *J. Am. Chem. Soc.* **1998**, *120*, 2415−2420.
(15) We have succeeded in revealing the reaction mechanism of the Diels−Alder and the related reactions for the synthesis of epoxyquinols and epoxytwinol A by DFT calculations: (a) Shoji, M.; Imai, H.; Shiina, I.; Kakeya, H.; Osada, H.; Hayashi, Y. *J. Org. Chem.* **2004**, *69*, 1548−1556. (b) Shiina, I.; Uchimaru, T.; Shoji, M.; Kakeya, H.; Osada, H.; Hayashi, Y. *Org. Lett.* **2006**, *8*, 1041−1044.
(16) All calculations were performed with the program package Spartan '10 1.1.0 of Wavefunction Inc. (http://www.wavefun.com). Cartesian coordinates and energy profiles for all reported structures are included in the Supporting Information.
(17) (a) Kawai, N.; Takao, K.; Kobayashi, S. *Tetrahedron Lett.* **1999**, *40*, 4193−4196. (b) Kawai, N.; Fujibayashi, Y.; Kuwabara, S.; Takao, K.; Ijuin, Y.; Kobayashi, S. *Tetrahedron* **2000**, *56*, 6467−6478. (c) Yamakoshi, S.; Hayashi, N.; Suzuki, T.; Nakada, M. *Tetrahedron Lett.* **2009**, *50*, 5372−5375. (d) Inoue, A.; Kanematsu, M.; Yoshida, M.; Shishido, K. *Tetrahedron Lett.* **2010**, *51*, 3966−3968. (e) Gärtner, M.; Kossler, D.; Pflästerer, D.; Helmchen, G. *J. Org. Chem.* **2012**, *77*, 4491−4495.
(18) (a) Nicolaou, K. C.; Liu, J.-J.; Yang, Z.; Ueno, H.; Sorensen, E. J.; Claiborne, C. F.; Guy, R. K.; Hwang, C.-K.; Nakada, M.; Nantermet, P. G. *J. Am. Chem. Soc.* **1995**, *117*, 634−644. (b) De Koning, H.; Subramanian-Erhart, K. E. C.; Huisman, H. O. *Synth. Commun.* **1973**, *3*, 25−28. (c) Yamazaki, N.; Dokoshi, W.; Kibayashi, C. *Org. Lett.* **2001**, *3*, 193−196 .
(19) Spectroscopic data on all compounds including AMF-26 (**1**) and AMF-14 (**2**) are included in the Supporting Information.
(20) (a) Dan, S.; Tsunoda, T.; Kitahara, O.; Yanagawa, R.; Zembutsu, H.; Katagiri, T.; Yamazaki, K.; Nakamura, Y.; Yamori, T. *Cancer Res.* **2002**, *62*, 1139−1147. (b) Yamori, T. *Cancer Chemother. Pharmacol.* **2003**, *52* (Suppl 1), S74−79. (c) Yaguchi, S.; Fukui, Y.; Koshimizu, I.; Yoshimi, H.; Matsuno, T.; Gouda, H.; Hirono, S.; Yamazaki, K.; Yamori, T. *J. Natl. Cancer Inst.* **2006**, *98*, 545−556. (d) Sharma, S. V.; Haber, D. A.; Settleman, J. *Nat. Rev. Cancer* **2010**, *10*, 241−253.
(21) (a) Paull, K. D.; Shoemaker, R. H.; Hodes, L.; Monks, A.; Scudiero, D. A.; Rubinstein, L.; Plowman, J.; Boyd, M. R. J. *Natl. Cancer Inst.* **1989**, *81*, 1088−1092. (b) Monks, A.; Scudiero, D.; Skehan, P.; Shoemaker, R.; Paull, K.; Vistica, D.; Hose, C.; Langley, J.; Cronise, P.; Vaigro-Wolff, A.; Gray-Goodrich, M.; Campbell, H.; Mayo, J.; Boyd, M. *J. Natl. Cancer Inst.* **1991**, *83*, 757−766. (c) Shoemaker, R. H. *Nat. Rev. Cancer* **2006**, *6*, 813−823.
(22) In the SAR studies of brefeldin A (BFA)-related compounds, there was another example in which an acylated BFA derivative possessing cell growth inhibitory activities does not disrupt the Golgi system. See ref 7.